Materials and Design 62 (2014) 233–240

Contents lists available at ScienceDirect

Materials and Design

journal homepage: www.elsevier.com/locate/matdes

Effects of dynamic mechanical properties on the ballistic performance of a new near-β titanium alloy Ti684

Rongting Li, Qunbo Fan *, Ruihua Gao, Lirui Huo, Fuchi Wang, Yangwei Wang

National Key Laboratory of Science and Technology on Materials under Shock and Impact, School of Materials Science and Engineering, Beijing Institute of Technology, Beijing 100081, China

ARTICLE INFO

Article history:
Received 19 January 2014
Accepted 21 May 2014
Available online 29 May 2014

Keywords:
New near-β titanium alloy
Dynamic mechanical property
Ballistic performance characterization methods

ABSTRACT

A comprehensive study of the newly developed near-β titanium alloy Ti684 has been carried out to determine the influence of the dynamic strength, dynamic hardness and critical failure strain on the ballistic impact properties. Two heat treatments of Ti684, namely β solution-treatment and α + β solution-treatment followed by aging, were carried out and the results were compared with Ti–6Al–4V. Ballistic impact tests were conducted on 7 mm thick front plates with a 20 mm thick A3 steel backing plate, using 7.62 mm armor piercing projectiles. The ballistic performance was evaluated by measuring the residual depth of penetration (DOP) in the A3 steel backing plates. It was found that the DOP values did not show obvious corresponding relation with both dynamic strength and dynamic hardness. The 800 °C solution +550 °C aged Ti684, which had the maximal dynamic strength, presented the worst ballistic performance, with a maximum DOP of 12.5 mm. In addition, the Ti–6Al–4V plate in the study with highest dynamic hardness did not show the best ballistic performance, having a DOP of 11.86 mm. However, as the critical failure strain increased, the DOP of the A3 steel backings were observed to decrease. This relationship was revealed from post ballistic microstructural observations.

1. Introduction

With the development of modern science and technology, the destructive power of anti-armor weapons is growing, and there has been growing demand for better materials. As titanium alloys have low density, high strength and excellent corrosion resistance, they have been widely used for airplanes and applications for armor materials for combat vehicles [1–3]. They have good mobility, transportability, and excellent ballistic performance, compared with high strength armor steel and light armor aluminum alloy. Ti–6Al–4V is widely used in armor applications. There are many reports describing the dynamic deformation behavior and microscopic damage mechanism of Ti–6Al–4V, prepared using various processing conditions, during ballistic impact [4–6]. Lee et al. [7] studied the effects of microstructural morphology on dynamic deformation behavior and ballistic impact properties of Ti–6Al–4V alloy with equiaxed and bimodal microstructures. Bar and Rosenberg [8] performed amount of ballistic tests to study the resistance to penetration of Ti6A14 V plates in different conditions and revealed that the copper sleeve, around the steel core, was very important in shearing a plug of material. Martinez et al. [9] studied the dynamic deformation Ti–6Al–4V targets with ballistic plug formation and fracture, impacted by a series of blunt, steel projectiles at velocities from 633 to 1027 m/s and found that the plugs of the targets were facilitated by horizontal and vertical adiabatic shear bands and cracks.

It is widely accepted that armor steels with relatively high strength and hardness show better performance in their ballistic impact resistance against small armor projectiles, under certain conditions [10–12]. Recently, the high-strength near β titanium alloy has been used for the development of new armor materials [13–15].

Fanning [16] studied the ballistic performance of different β-Ti alloys against 7.62 mm armor piercing projectiles. Unfortunately, the β-Ti alloy with high strength did not show better ballistic resistance than the Ti–6Al–4V, as a result of severe spalling of the backing. Sukumar et al. [17] carried out a study of the ballistic impact behavior of a high strength metastable near β-Ti alloy. The test was carried out on a number of 10 mm near β-Ti alloy plates, of different microstructural properties, with 50 mm thick 7017 Al alloy backing, against 7.62 mm armor piercing projectiles. The depth of penetration (DOP) in the backing plate was measured to evaluate the ballistic resistance. They showed that the as-rolled near β-Ti alloy and the same alloy treated with α + β solution then aged produced no better ballistic performance than the original

* Corresponding author. Tel.: +86 10 68911144 863; fax: +86 10 68911144 866.
E-mail address: fanqunbo@bit.edu.cn (Q. Fan).

http://dx.doi.org/10.1016/j.matdes.2014.05.044
0261-3069/

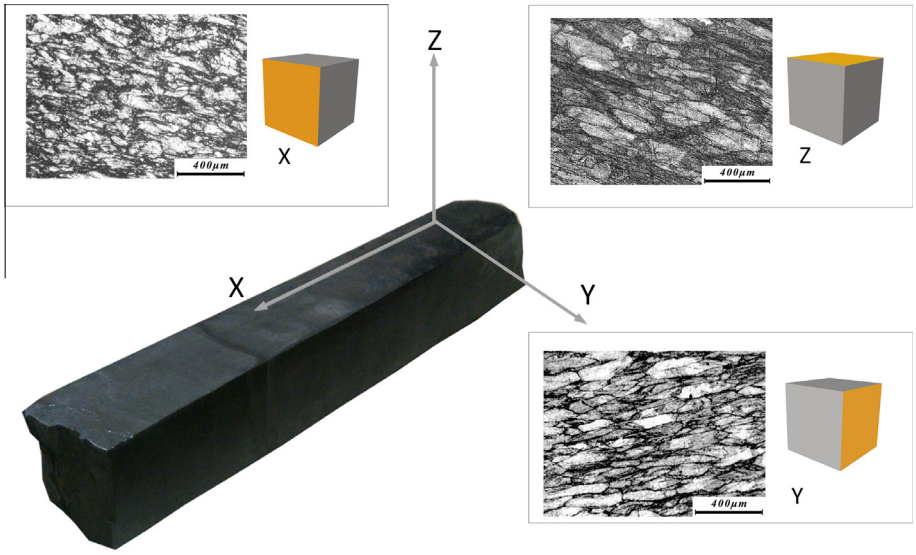

Fig. 1. Microstructure of the free forged billet.

Table 1
Chemical composition (wt%) of the Ti684 alloy.

Element	Al	Mo	Cr	Fe	Si	O	N
Wt (%)	6.04	8.02	3.99	0.59	0.35	/	/

Ti–6Al–4V, despite the higher static strength, hardness and ductility, as measured in quasi-static tests. The results showed that none of the static mechanical properties had predicted the residual depth of penetration.

However, the static mechanical tests are under rather low strain-rate loading conditions, usually bellow 10^{-2} s^{-1}. Problems arise as to whether the static mechanical test techniques can be extended to evaluate material performance under dynamic loading conditions. Note that the high strain-rate testing conditions for dynamic mechanical properties are similar to high-speed impacts in a practical environment for armor material, so it is of great significance to study the relationship between the dynamic mechanical properties and the ballistic impact behavior of high-strength β-Ti alloys.

The present study is performed on a new near β titanium alloy Ti684 developed at the Beijing Institute of Technology. The design criterion is mainly based on high dynamic strength and high dynamic ductility. Targets in different microstructural conditions, with moderate combinations of high dynamic strength, high hardness and critical failure strain, are selected to carry out ballistic impact tests and compare results with standard Ti–6Al–4V. The influence of dynamic mechanical properties on the ballistic performance is discussed and microstructure observation is used to analyze the microscopic mechanism.

2. Experimental details

The Ti684 alloy used in the current study was produced by melting the raw alloy in a vacuum arc furnace. The billet was then forged into square pieces by repeatedly upsetting and stretching to ensure the homogeneity. The microstructure in *X*, *Y* and *Z* normal directions are shown in Fig. 1, indicating that the forged piece does feature a homogeneous structure. The chemical composition of the alloy is given in Table 1. Differential thermal analysis was carried out, and the beta-transus temperature of Ti684 alloy was found to be 855 °C ± 5 °C. The heat treatments, including the T_β annealing noted above and the T_β bellow solution and aging, are shown in Table 2. The reference Ti–6Al–4V sample used in the study was supplied by Baoji Non-ferrous Metal Processing Plant, China.

The dynamic compression tests were performed using the Spilt Hopkinson Pressure Bar (SHPB) system [18–20] in Fig. 2. Tests

Table 2
Heat treatment conditions used in the present study.

No.	Material	β Transus temperature (°C)	Heat treatment
1	Ti684	855 ± 5	800 °C/2 h/water quenching (WQ) + 550 °C/4 h/WQ
2	Ti684	855 ± 5	900 °C/15 min/WQ
3	Ti684	855 ± 5	760 °C/2 h/air cooling (AC) + 550 °C/6 h/AC
4	Ti6Al4 V	975 ± 5	Supplied

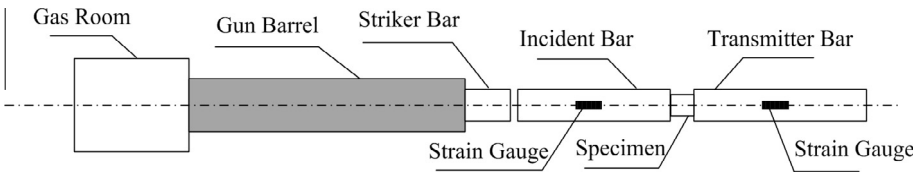

Fig. 2. Configuration of SHPB test.

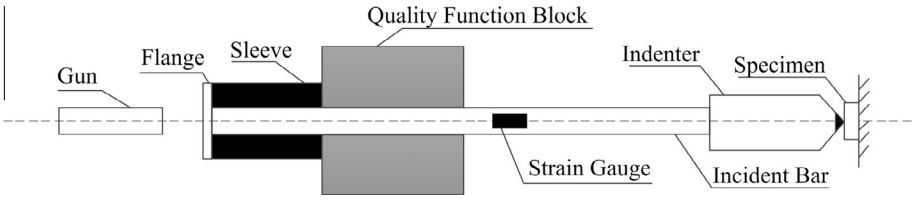

Fig. 3. Configuration of dynamic indentation hardness test.

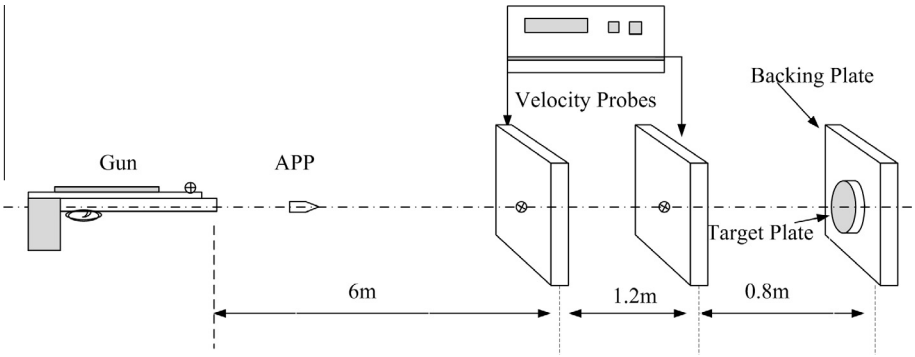

Fig. 4. Configuration of ballistic impact test.

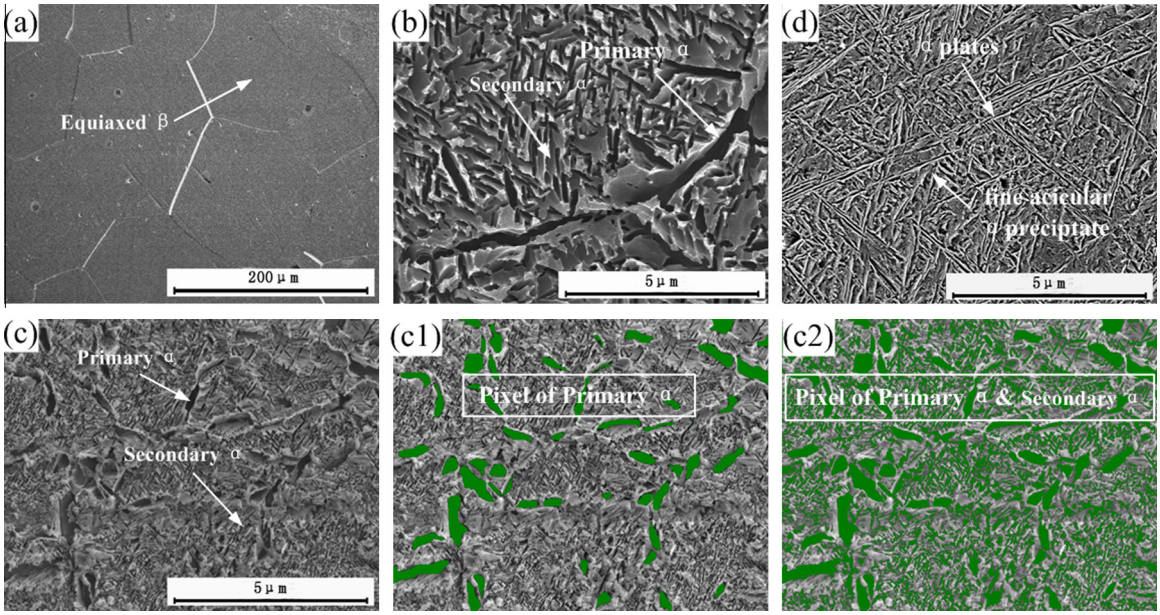

Fig. 5. Microstructure of Ti684 and Ti–6Al–4V plates in different conditions in (a) 900 °C WQ, (b) 760 °C STA, (c) 800 °C STA, (c1) primary α in 800 °C STA sample, (c2) primary α and secondary α in 800 °C STA sample and (d) Ti–6Al–4V.

were carried out on cylindrical samples with a diameter of 5 mm and a height of 5 mm. The true dynamic compression stress–strain curves at high strain rate was calculated from engineering stress and strain switched from the original pulses of incident, reflected and transmitted waves collected by the data acquisition system.

The dynamic indentation hardness test was conducted using a dynamic indentation hardness measuring system developed independently by the Beijing Institute of Technology (Fig. 3) [21]. The test was conducted on a smooth and polished cuboid with size $15 \times 15 \times 5$ mm. The voltage–time signal was collected by a pressure transducer and transformed into the surge pressure peak value after calibrating. The dynamic Vickers hardness (DHV) was calculated from the surge pressure peak value, using the following formula:

$$\mathrm{DHV} = 2(P_d/9.8) \cdot (\sin\alpha/2)/d^2 = 0.1892P_d/d^2 \quad (1)$$

where P_d is the stress pulse peak under dynamic loading (N) and d is the average of the dynamic indentation diagonals (mm).

The ballistic tests were performed in the Institute of Mechanics, Chinese Academy of Science. The setup for the ballistic impact test is shown in Fig. 4. The tests were carried out on a range of 7 mm thick Ti684 plates with different microstructural properties, with a 20 mm thick A3 steel backing, and using 7.62 mm armor piercing

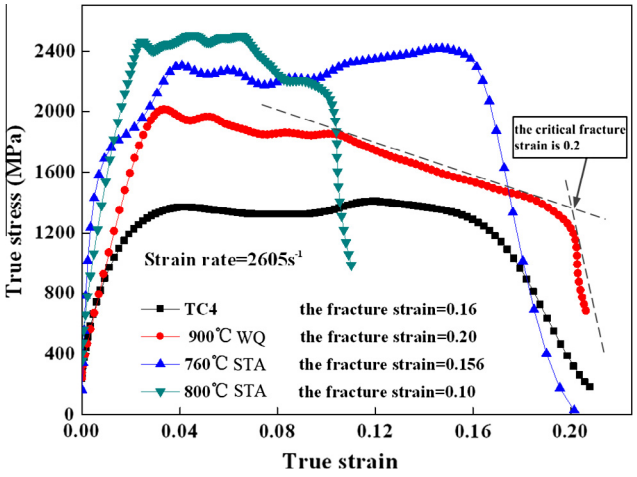

Fig. 6. Stress–strain curves obtained from the dynamic compression test of all conditions.

projectiles (APP). The velocity of the projectile was measured between two screens of velocity probes, through which the time when the bullet successively penetrates two screens and the distance were recorded by the data acquisition system. The resolution of the time data acquisition system is 10^{-6} s. The DOP in the 20 mm thick A3 steel backing was measured in order to evaluate the ballistic resistance.

The microstructures of specimens were observed using the scanning electron microscopy (SEM) and the optical microscopy (OM). X-ray diffraction (XRD) analysis for phase identification were conducted on a Rigaku Smartlab diffractometer. Specimens for microstructure studies and X-ray analysis are treated by electrochemical polishing in a 95% ethanoic acid + 5% perchloric acid, and etched with a 4% HF + 8%HNO_3 + 88%H_2O solution at room temperature.

3. Results and discussion

3.1. Microstructures

The microstructures of the various Ti684 alloys and Ti–6Al–4V are shown in Fig. 5. The microstructure of the sample prepared using the 900 °C WQ conditions (Fig. 5(a)) consists of equiaxial β grains. The micrograph of the 900 °C WQ sample shows large grains, with an average size of ~150 μm. The microstructure of the Ti–6Al–4V sample (Fig. 5(d)) is near the basket wave structure. The microstructures of the 760 °C solution treated and aged (STA) sample (Fig. 5(b)) consists of elongated primary α grains formed during the solution treatment, together with fine secondary α grains formed during the aging treatment in the transformed β matrix. The microstructure of the 800 °C solution treated and aged (STA) sample (Fig. 5(c)) is nearly the same as the 760 °C STA, and Image-Pro Plus is used to perform quantitative image analysis to determine the volume fraction of each phase of the 760 °C STA

Table 3
Dynamic hardness of all conditions.

Material	Condition	Dynamic hardness (DHV)	Dynamic YS (MPa)
Ti684	900 °C/15 min/WQ	515 ± 10	1870 ± 50
	760 °C/2 h/AC + 550 °C/6 h/AC	733 ± 5	2200 ± 60
	800 °C/2 h/WQ + 550 °C/4 h/WQ	710 ± 6	2400 ± 80
Ti6Al4 V	Supplied	737 ± 6	1370 ± 50

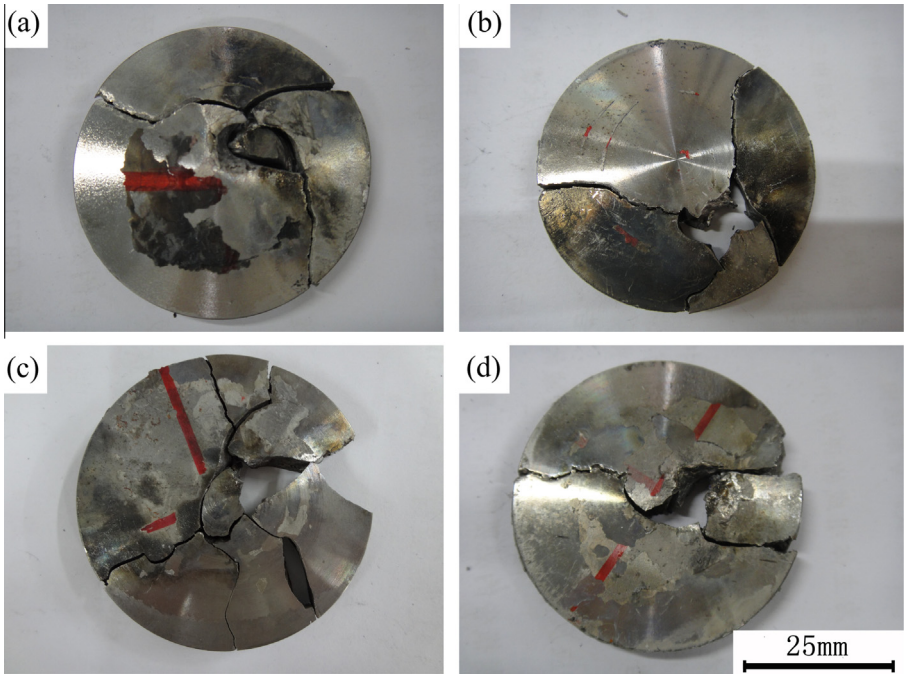

Fig. 7. Damage situation of titanium alloy target of all conditions. (a) 900 °C WQ, (b) 760 °C STA, (c) 800 °C STA and (d) Ti–6Al–4V.

Table 4
Dynamic mechanical properties and the ballistic properties of all conditions.

Material	Condition	DOP (mm)	Dynamic YS (MPa)	Critical fracture strain (%)
Ti684	900 °C/15 min/WQ	8.86 ± 0.04	1870 ± 50	20 ± 0.2
	760 °C/2 h/AC + 550 °C/6 h/AC	11.98 ± 0.02	2200 ± 60	15.6 ± 0.2
	800 °C/2 h/WQ + 550 °C/4 h/WQ	12.52 ± 0.02	2400 ± 80	10 ± 0.2
Ti6Al4 V	Supplied	11.86 ± 0.02	1370 ± 50	16 ± 0.2

and 800 °C STA condition. The pixel numbers occupied by each phase can be identified and counted by this software automatically, thus approximately representing the volume fraction of each phase. As shown in Fig. 5(c1) and (c2), primary α and secondary α for 800 °C STA sample are colored in green[1], and the volume fractions can then be calculated. At least three microstructures for each condition were tested to ensure the reliability of the statistic values. The results show that the 800 °C STA condition microstructure presents 5.4% of primary α and 59.49% of secondary α. The 760 °C STA condition microstructure presents 9.3% of primary α and 37.2% of secondary α. Due to the higher solution temperature, the 800 °C STA sample has a lower volume fraction of the primary α and a higher volume fraction of fine secondary α.

3.2. Dynamic mechanical properties

The function of the armor target in a real service environment is usually to resist high speed penetration [22], so it is of great importance to study the dynamic behavior of the armor titanium alloy in the high strain rate condition of the dynamic test.

Fig. 6 shows the dynamic true stress–strain curves of all the Ti684 alloy samples and Ti–6Al–4V at a strain rate of 2605 s^{-1}. Considering the saw tooth form of the curves, the dynamic strength is determined by the steady-state plastic flow stress, and the critical fracture strain is determined by the intersection point between two tangent lines with regard to the plastic flow stress and the collapsed-stage stress. As an example illustrated in Fig. 6, the critical fracture strain of 900 °C WQ sample is 0.2. It can be seen that all the Ti684 samples have higher dynamic strength than the Ti–6Al–4V sample supplied. This is a result of the solid solution strengthening effect attributed to high content of the stable β phase elements in Ti684.The dynamic yield strength of the 800 °C STA sample is 2400 MPa and the critical fracture strain is 0.1. The 760 °C STA condition has a lower dynamic yield strength than the 800 °C STA, about 2200 MPa, with a critical fracture strain of 0.156. This can be explained by the larger volume fractions of fine secondary α in the 800 °C STA sample [23]. Finally, the 900 °C WQ sample has a maximal critical fracture strain of 0.20 and a dynamic yield strength of 1870 MPa.

In this study, dynamic hardness tests were performed using the dynamic indentation hardness measuring system. At least 3 samples were tested for each microstructural condition. The average value of dynamic hardness and dynamic strength of all test samples are shown in Table 3 along with their standard deviations. The 800 °C STA sample has the highest dynamic strength, 2400 MPa, with a stand deviation of 80 MPa and a dynamic hardness of 710 DHV, with a stand deviation of 6 DHV. The Ti–6Al–4V sample has the lowest dynamic strength, 1370 MPa, with a stand deviation of 50 MPa but shows the highest dynamic hardness, 737 DHV with a stand deviation of 6 DHV. Therefore, no obvious corresponding relationship is observed between the dynamic strength and the dynamic hardness. Different stress conditions during the two dynamic mechanical tests may contribute to the

[1] For interpretation of color in Fig. 5, the reader is referred to the web version of this article.

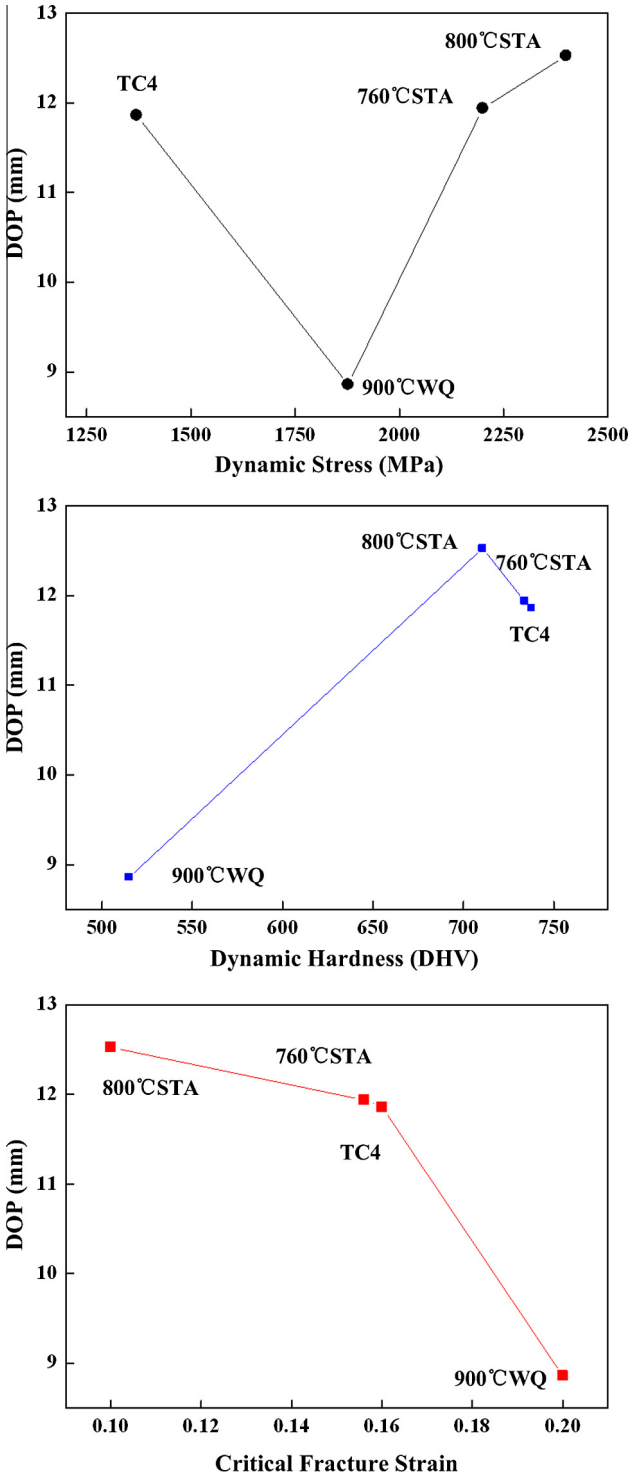

Fig. 8. Effect of dynamic mechanical properties on depth penetration.

results since the dynamic strength is obtained under dynamic uniaxial compression [24], but the plastic deformation and damage during the dynamic hardness test is attributed to the complex three-dimensional stress arising from the particular loading of the metal. The dynamic hardness is a measure of the resistance to deformation and damage [22].

3.3. Ballistic performance study

Fig. 7 shows the damage observed for different target plates. It can be seen that the plates of the Ti684 900 °C WQ sample (Fig. 7(a)) and Ti–6Al–4V (Fig. 7(d)) both break into three parts, the 760 °C STA sample (Fig. 7(b)) into four parts. The 800 °C STA sample (Fig. 7(c)) is the most seriously damaged, breaking into seven parts.

The dynamic mechanical properties, namely critical fracture strain, dynamic hardness and ballistic test results for all samples, are summarized in Table 4 along with their standard deviations. Combining Fig. 7 with Table 4, it is clear that the most seriously damaged 800 °C STA target has the deepest DOP of 12.52 mm, with a stand deviation 0.02 mm and shows the worst ballistic performance. The 900 °C WQ sample has the minimum DOP of 8.86 mm, with a stand deviation of 0.04 mm and shows the best ballistic performance. The 760 °C STA sample and Ti–6Al–4V have similar residual depths.

In order to further study the relationship between the dynamic mechanical properties and the ballistic impact properties, the values of DOP as functions of dynamic strength, critical fracture strain, and dynamic hardness are shown in Fig. 8. Analysis of Fig. 8(a) shows that, as the dynamic strength increases from 1370 MPa (Ti–6Al–4V) to 2200 MPa (900 °C WQ), the residual depth of penetration in the A3 backing plate decreases from 11.86 mm to 8.86 mm. Subsequently, with further increase in dynamic strength from 2200 MPa (760 °C STA) to 2400 MPa (800 °C STA), the DOP of the backing plate increases to 11.98 mm and 12.52 mm, respectively. Therefore, the DOP shows an initial increase with dynamic strength then a reduction. There appears to be no clear relationship between the dynamic strength and the residual depth of penetration in the backing plate.

In the curve of DOP vs. dynamic hardness, Fig. 8(b), the DOP first increases from 8.86 mm (900 °C WQ) to 12.52 mm (800 °C STA) as the dynamic hardness increases from 515DHV (900 °C WQ) to 710DHV (800 °C STA). Then, as the dynamic hardness increases to 733 DHV (760 °C STA) and 737 DHV (Ti–6Al–4V), the DOP is once again reduced. Therefore, there is no clear correlation between dynamic hardness and the DOP, either.

However, in Fig. 8(c), the 800 °C STA sample with the minimum critical fracture strain 0.1 shows the worst ballistic performance, with the maximum DOP of 12.52 mm. As the critical fracture strain increases to 0.156 (760 °C STA) and 0.160 (Ti–6Al–4V), the DOP decreases to 11.98 mm and 11.86. The 900 °C WQ sample with the maximum critical fracture strain of 0.2 shows the best ballistic performance, with the minimum DOP value of 8.86 mm. These results show that below a particular value of dynamic strength, as the critical fracture strain increases, the residual depth of penetration in the A3 backing plate decreases, indicating that the higher dynamic plasticity attributes to better ballistic impact performance.

The SEM fractographs of the impact fracture surfaces of all samples are shown in Fig. 9. The 900 °C WQ sample (Fig. 9(a)), the 760 °C STA sample (Fig. 9(b)) and Ti–6Al–4V (Fig. 9(d)) all show typical ductile fracture modes, with some ductile dimples, revealing that the target plates have experienced obvious macroscopic plastic deformation before fracture, which can also be induced from the critical fracture strain values illustrated in Fig. 6 and Table 4. In Fig. 9(c), the 800 °C STA samples exhibits brittle fracture, with little dimple fracture, indicating that the fracture of the 800 °C STA sample is mainly of the brittle fracture type. The 900 °C WQ sample impact fracture shows the largest region of dimples. Large amounts of energy are consumed during the tearing process in ductile fracture, so under the high speed impact of the armor piercing projectiles, the ductile fracture process consumes more energy and the target plate with better ductile fracture properties shows better ballistic impact performance. Further studies show that quite a few of the acicular martensites α'' are found only in the microstructure of the crater cross section of 900 °C/15 min/WQ Ti684 (Fig. 10(a)), which are also confirmed by the X-ray scan result (Fig. 10(b)). Many studies [25–27] have revealed that the

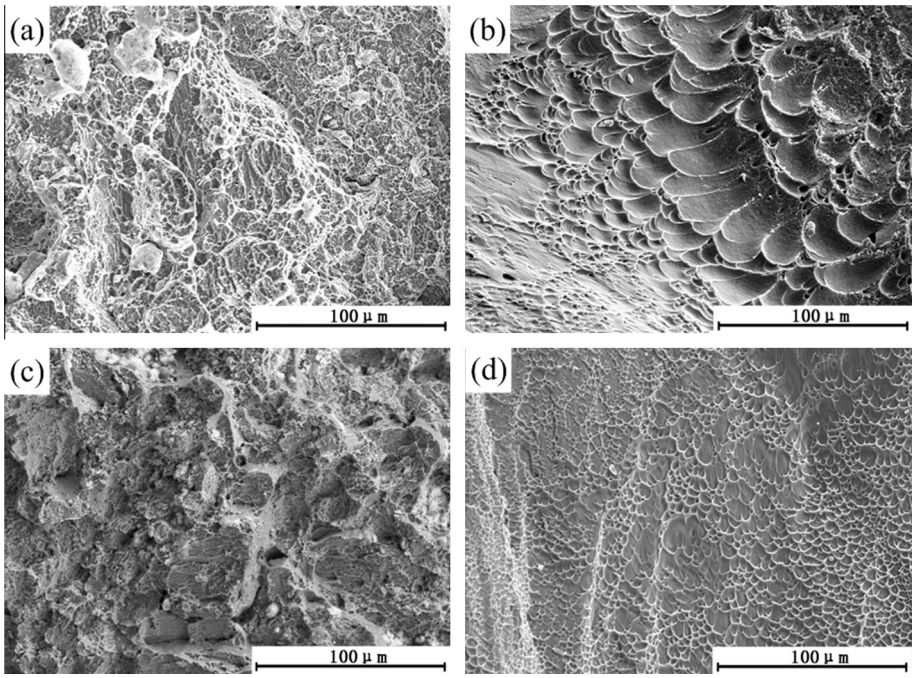

Fig. 9. Impact fracture surfaces (a) 900 °C WQ, (b) 760 °C STA, (c) 800 °C STA and (d) Ti–6Al–4V.

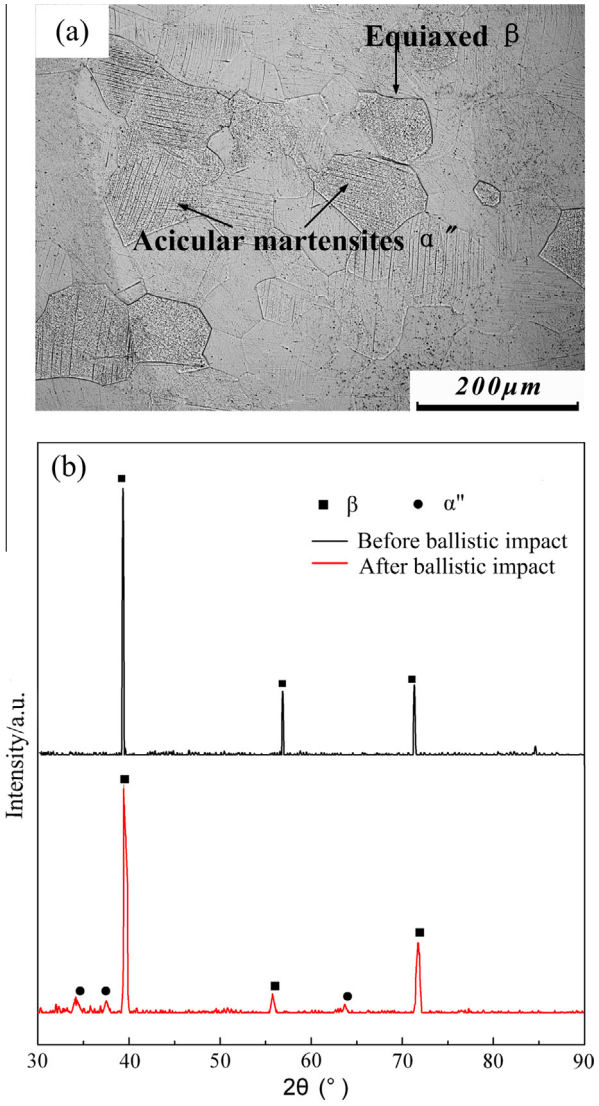

Fig. 10. (a) Optical microstructure of the crater cross section of 900 °C WQ Ti684 and (b) XRD pattern of the 900 °C WQ Ti684 sample before and after ballistic impact.

stress-induced martensite transformation improved the strain-hardening effect and slowed down the growth of the crack and fracture, which increased the toughness of the material and improves the ballistic performance. Consequently, the 900 °C WQ sample has the best ballistic impact performance of all, matching the relatively larger critical fracture strain.

4. Conclusions

The effect of dynamic mechanical properties on the ballistic performance of a new near-β titanium alloy Ti684 is studied. Dynamic mechanical tests, including a dynamic compression test and a dynamic indentation hardness test, are carried out to study the influence of the dynamic mechanical properties on the ballistic performance and to compare with Ti–6Al–4V. The near β titanium alloy Ti684 showed high dynamic strength and dynamic hardness, but neither of the two dynamic mechanical properties exactly predicted the ballistic performance. However, under a particular value of dynamic strength, as the critical fracture strain increased, the DOP in the A3 steel backing also decreased, indicating that the higher dynamic ductility in the critical fracture strain contributed to better ballistic performance. The stress-induced martensite is found in the ballistic impact progress of the 900 °C WQ Ti684 plate, which slows down the growth of the crack and fracture, increases the toughness of the material, thus improving the ballistic performance of material to some extent.

Acknowledgement

We gratefully acknowledge the financial support of the program for New Century Excellent Talents in University (NCET-12-0051).

References

[1] Whittaker MT, Harrison W, Hurley PJ, Williams S. Modeling the behavior of titanium alloys at high temperature for gas turbine applications. Mater Sci Eng A 2010;527(16–17):4365–72.
[2] MacDonald DE, Rapuano BE, Deo N, Stranick M, Somasundaran P, Boskey AL. Thermal and chemical modification of titanium–aluminum–vanadium implant materials: effects on surface properties, glycoprotein adsorption, and MG63 cell attachment. Biomaterials 2004;25(16):135–3146.
[3] Niinomi M. Mechanical properties of biomedical titanium alloys. Mater Sci Eng A 1998;243(1–2):231–6.
[4] Nesterenko VF, Goldsmith W, Iindrakanti SS, YaBei G. Response of hot isostatically pressed Ti–6Al–4V targets to normal impact by conical and blunt projectiles. Int J Impact Eng 2003;28:137–60.
[5] Kad BK, Schoenfeld SE, Burkins MS. Computational modeling of through-thickness dynamic impact response in cross-rolled Ti–6Al–4V plates. Mater Sci Eng A 2002;322(3):41–51.
[6] Semiatin SL, Bieler TR. Effect of texture and slip mode on the anisotropy of plastic flow and flow softening during hot working of Ti–6Al–4V. Metall Mater Trans A 2001;32(17):1871–5.
[7] Lee DG, Lee S, Lee CS, Hur SM. Dynamic deformation behavior and ballistic impact properties of Ti–6Ale–4V alloy having equiaxed and bimodal microstructures. Metall Mater Trans A 2003;34:2541–8.
[8] Bar YM, Rosenberg Z. On the correlation between the ballistic behavior and dynamic properties of titanium-alloy plates. Int J Impact Eng 1997;19(4):311–8.
[9] Martinez F, Murr LE, Ramirez AC, Lopez MI, Gaytan SM. Dynamic deformation and adiabatic shear microstructures associated with ballistic plug formation and fracture in Ti–6Al–4V targets. Mater Sci Eng A 2007;454–455:581–9.
[10] Borvik T, Dey S, Clausen AH. Perforation resistance of five different high-strength steel plates subjected to small-arms projectiles. Int J Impact Eng 2009;36:948–64.
[11] Dey S, Borvik T, Hopperstad OS, Leinum JR, Langseth M. The effect of target strength on the perforation of steel plates using three different projectile nose shapes. Int J Impact Eng 2004;30(8–9):1005–38.
[12] Dikshit SN, Kutumbarao VV, Sundararajan G. The influence of plate hardness on the ballistic penetration of thick steel plates. Int J Impact Eng 1995;16(2):293–320.
[13] Fanning JC. Military applications for β titanium alloys. J Mater Eng Perform 2005;14(6):686–90.
[14] Burkins MS, Hansen JS, Paige JI. The effect of thermo-mechanical processing on the ballistic limit velocity of extra low interstitial titanium alloy Ti–6Al–4V. Aberdeen Proving ground (MD): Army Research Laboratory; 2000. p. 1–69. ARL-MR-486.
[15] Batus SD. Evaluation of titanium–5Al–5Mo–5V–3Cr (Ti-5553) alloy against fragment and armor-piercing projectiles. Aberdeen Proving ground (MD): Army Research Laboratory; 2009. p. 1–34. RL-TR-4996.
[16] Fanning JC. Effectiveness of timetal-15-3 as armor against small arms Non aerospace applications of titanium. Warrendale (PA): TMS; 2003. p. 297–304.
[17] Sukumar G, Bhav Singh B, Bhattacharjee A, Siva Kumar K, Gogia AK. Ballistic impact behavior of β-CEZ Ti alloy against 7.62 mm armour piercing projectiles. Int J Impact Eng 2013;54:149–60.
[18] Peirs J, Verleysen P, Degrieck J, Coghe F. The use of hat-shaped specimens to study the high strain rate shear behavior of Ti–6Al–4V. Int J Impact Eng 2010;37(6):703–14.
[19] Andrade U, Meyers MA. Dynamic recrystallization in high-strain, high-strain-rate plastic deformation of copper. Acta Metall Mater 1994;42(9):3183–95.
[20] Chen YC, Nakata K. Microstructural characterization and mechanical properties in friction stir welding of aluminum and titanium dissimilar alloys. Mater Des 2009;30(3):469–74.
[21] Yangwei W, Zhuang M, Xiaodong Y, Fuchi W, Xin H. Dynamic indentation hardness of typical materials. Mater Eng 2010;9:62–6.
[22] Montgomer JS, Wells MGH. Low-cost titanium armors for combat vehicles. JOM 2001;49(5):29–32.
[23] Peng G, Yongqing Z, Lian Z. Influence of solution conditions on aging response of a new metastable beta titanium alloy. Rare Met Mater Eng 2006;35(5):707–10.

[24] Meng H, Li QM. Correlation between the accuracy of a SHPB test and the stress uniformity based on numerical experiments. Int J Impact Eng 2003;28(5):537–55.
[25] Grosdidier T, Philippe MJ. Deformation induced martensite and superelasticity in a β-metastable titanium alloy. Mater Sci Eng A 2000;291:218–23.
[26] Neelakantan S, San Martin D, Rivera-Díaz-del-Castillo PE. Design of titanium alloys showing plasticity induced transformation. J Mater Sci Technol 2009;25:1358.
[27] Kharia KK, Rack HJ. Martensitic phase transformations in IMI 550. Metall Mater Trans A 2001;32:679.